Acta Mech. Sin. (2011) 27(6):1013–1022
DOI 10.1007/s10409-011-0507-z

RESEARCH PAPER

Micromechanical analysis of the behavior of stiff clay

Zhen-Yu Yin · Ching S. Chang · Pierre-Yves Hicher · Jian-Hua Wang

Received: 6 August 2010 / Revised: 14 March 2011 / Accepted: 19 July 2011

Abstract Cementations formed in geological timescale are observed in various stiff clays. A micromechanical stress strain model is developed for modeling the effect of cementation on the deformation behavior of stiff clay. The proposed approach considers explicitly cementations at inter-cluster contacts, which is different from conventional model. The concept of inter-cluster bonding is introduced to account for an additional cohesion in shear sliding and a higher yield stress in normal compression. A damage law for inter-cluster bonding is proposed at cluster contacts for the debonding process during mechanical loading. The model is used to simulate numerous stress-path tests on Vallericca stiff clay. The applicability of the present model is evaluated through comparisons between the predicted and the measured results. In order to explain the stress-induced anisotropy arising from externally applied load, the evolution of local stresses and local strains at inter-cluster planes are discussed.

The project was supported by the Shanghai Pujiang Talent People Project (11PJ1405700), and the National Science Funds for Distinguished Young Scholars (51025932).

Z.-Y. Yin (✉) · J.-H. Wang
Department of Civil Engineering,
Shanghai Jiao Tong University,
200240 Shanghai, China
e-mail: zhenyu.yin@gmail.com

C.-S. Chang
Department of Civil and Environmental Engineering,
University of Massachusetts,
Amherst, MA 01002, USA

P.-Y. Hicher
Research Institute in Civil and Mechanical Engineering,
UMR CNRS 6183, Ecole Centrale de Nantes,
BP 92101, 44321 Nantes, France

Keywords Stiff clay · Destructuration · Micromechanics · Plasticity · Induced anisotropy

1 Introduction

Mechanical behavior of stiff clay has been widely studied experimentally during last decades [1–9]. In general, the reconstituted clay was used as a reference for interpreting the behavior of natural soil. The observed differences were attributed to structure, defined as the combination of particle arrangement (fabric) and inter-particle bonding.

Microstructure investigations on several stiff clays were reported in the literature. Different from soft structured clay (with bigger void ratio than reconstituted sample), stiff clays have soil structure with small void between clusters (smaller void ratio than reconstituted sample). In addition to the formation of particle arrangement, carbonates were also found within a matrix of stiff clay. For instance, there is about 26.5% of carbonate content in Todi clay [2], 22% in Pappadai clay [3], 25% – 40% in stiff Pleistocene clay [6], 20% in stiff North Sea clay [8], 30% in Vallericca clay [9]. These carbonates were found to be extremely fine and possibly to be responsible for inter-particle or inter-cluster (aggregate of particles) bonding, as indicated by researchers [2, 3, 6, 8–10]. This bonding might be formed during clay deposition history on a geological timescale. Experimental evidence also shows a mechanical bond degradation (de-bonding) process during applied mechanical loading. This bond degradation is an irreversible phenomenon that, experimentally, appears to be controlled by plastic strain accumulation [10].

The behavior of stiff clay was modeled by conventional elasto-plastic models [11–14]. In these approaches, the material structure, including fabric and bonding, was accounted for by the initial size of yield surface in a stress space. A damage-type mechanism was introduced which permits reduction of the size of the yield surface due to bond degra-

dation. However, the bonding and debonding at the inter-cluster contact level has not been explicitly considered in these models.

In order to tackle this issue, the micromechanics approach [15–17] is adopted here. In this approach, the clay is regarded as an assembly of clusters (aggregates of clay particles). The deformation of an assembly can be obtained by integrating the movement of the inter-cluster contacts in all orientations. Thus, the effect of inter-cluster bonding can be explicitly represented by adopting the general assumption of presence of inter-cluster bonding. Since the orientation dependent properties of soil are explicitly represented, the induced anisotropy can be modeled in a more direct way [16,17]. Therefore, the proposed approach is of more physical significance than conventional one.

In this paper, the destructuring behavior of stiff clays is first described. Based on this, we extend the micromechanical model [15] by introducing inter-cluster bonding and debonding at the contact plane level: the inter-cluster bonding increases both the shear strength and normal compression strength, and an inter-cluster debonding model is used to describe the bond degradation process subjected to mechanical loading. The model is then employed to simulate triaxial tests with various stress paths on stiff Vallericca clay for verification of this approach. The evolution of local stresses and local strains at inter-cluster planes due to externally applied load are also discussed which demonstrates different behaviors of contact planes with various orientations. The overall applicability of the present model is evaluated based on the comparison between measured and predicted results.

2 Experimental investigation

2.1 Bonding and debonding effect on compression behavior

Figure 1 shows the compression curves in e–σ'_v (void ratio versus vertical effective stress) plane from oedometer tests on both intact and reconstituted samples of four stiff clays [2]. It can be concluded from comparing the results of intact samples with those of reconstituted samples that the inter-cluster bonding due to cementation results in a significant increase of compression yield stress.

For compression behavior, when the applied loads reach the yield stress, a mechanical bond degradation process is initiated (see Fig. 1). The inter-cluster bonds are progressively lost, and the rate of debonding is different for different types of clay (e.g., rapid degradation in Pietrafitta clay in Fig. 1a). It needs to be noticed that, even at large strains and high stress levels during one-dimensional compression, the compression curves do not merged to that of the reconstituted clay. This indicates that there are still enough bonds exist for stiff clay. This phenomenon is different from soft sensitive clay in which the bonds are easily destroyed so that it behaves as a fully reconstituted material very soon after the compression load exceeds its yield stress.

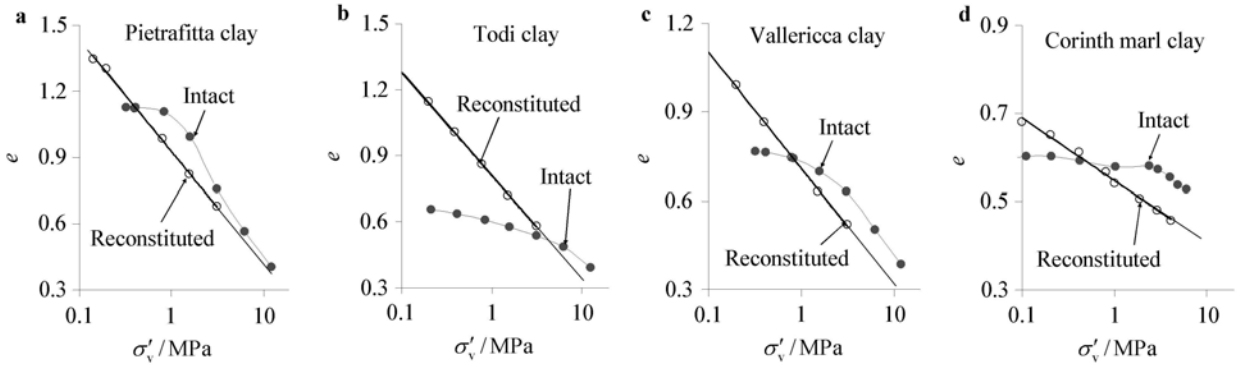

Fig. 1 Experimental results of oedometer test on intact and reconstituted samples of stiff clays

2.2 Bonding and debonding effect on shear behavior

Burland et al. [2] plotted peak strengths in p'-q (mean effective stress versus deviatoric stress) plane for both reconstituted and intact samples of four stiff clays. For stiff clays under over-consolidated condition, the slope of peak strength of intact samples is generally parallel to and higher than that of reconstituted samples (see Fig. 2a). This difference of peak strength between intact and reconstituted samples can also be found on stiff clays under normally consolidated and slightly overconsolidated condition, as shown in Fig. 2b for Pleistocene clay [6], and in Fig. 2c for Vallericca clay [9] etc. This difference of peak strength is attributed to inter-cluster bonding.

Upon increase of the applied shear loads, the inter-cluster bonds are progressively lost. As a result, decrease of deviatoric stress after peak value takes place for intact samples of stiff clays, as shown in Figs. 2b and 2c.

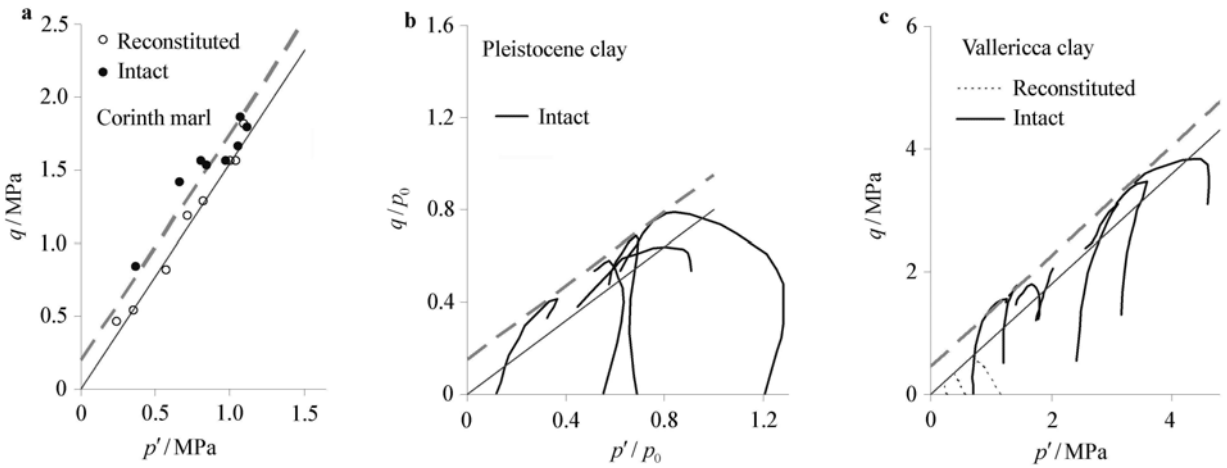

Fig. 2 **a** Peak strength of intact and reconstituted samples of stiff clay; **b**, **c** Effective stress paths from triaxial test on intact and reconstituted samples of stiff clays

3 Micromechanical stress strain model

Based on the bonding and debonding effect on mechanical behavior of stiff clay, a micromechanical modeling method is proposed. The model is extended from the clay model by Chang et al. [15]. Only the modification to account for the effect of inter-cluster bonding and debonding is discussed below.

3.1 Inter-cluster behavior

3.1.1 Shear sliding

In order to take into account the effect of inter-cluster bonding, the plastic law of shear sliding at inter-cluster contacts [15] is modified. The yield function for shear sliding is assumed to be of Mohr–Coulomb type, defined in a contact-stress space (e.g. σ, τ_s, τ_t defined in Ref. [15], see coordinate system shown in Fig. 3), as follows

$$F_1(\sigma, \tau, \sigma_b, H_1) = \frac{\tau}{\sigma + \sigma_b} - H_1(\gamma^p), \tag{1}$$

where σ_b is the inter-cluster cohesion due to inter-cluster bonding, $H_1(\gamma^p)$ is a hardening/softening function. For a given value of σ_b, the failure line τ/σ can shift to left with a distance of σ_b, as shown in Fig. 2, which gives the initial amount of inter-cluster bonds. For $\sigma_b = 0$, Eq. (1) can be reduced to that used in Ref. [15].

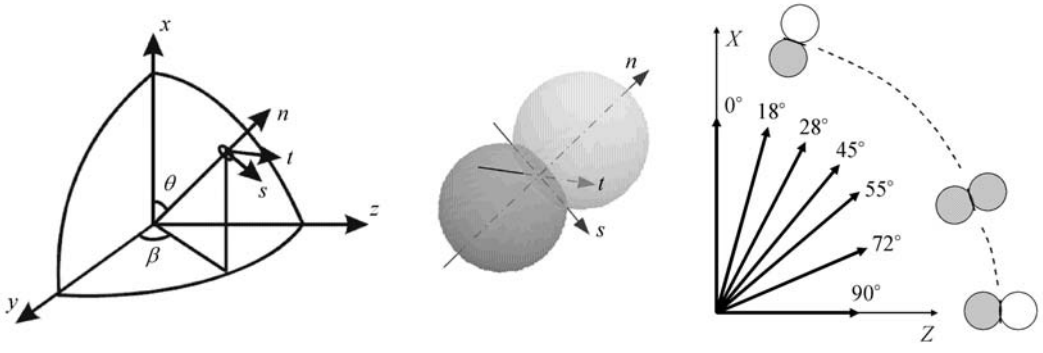

Fig. 3 Local coordinate at inter-particle contact

The stress dilatancy of stiff clay were reported [3, 8], which can be described by Taylor's dilatancy equation. According to these observations, the local dilatancy equation is assumed in the same form as Taylor's equation, given by

$$\frac{d\varepsilon^p}{d\gamma^p} = D(\tan\phi_0 - \tan\phi_m), \tag{2}$$

where $\tan\phi_m = \tau/(\sigma + \sigma_b)$; D is a material constant for stress dilatancy. In Eq. (2), the $\tan\phi_0$ also represents the slope of the phase transformation line [18], at which the plastic volumetric strain rate is zero.

The degradation of inter-cluster bonds can be modeled as a damage of the bonded contacts. Therefore, a damage law was introduced in the expression of the inter-cluster co-

hesion, expressed as

$$\sigma_{\mathrm{b}} = \sigma_{\mathrm{b0}} \exp(-\xi_{\mathrm{d}} \gamma^{\mathrm{p}}), \tag{3}$$

where σ_{b0} is the initial inter-cluster cohesion; ξ_{d} is the factor of damage representing the influence of the tangential displacement in the damage law. Therefore, during loading each contact produces a progressive damage of cohesion.

3.1.2 Normal compression

In order to account for inter-cluster bonding effect on the compression behavior of stiff clay, the second plastic law for normal compression of inter-cluster contact [15] is modefied as

$$F_2(\sigma, \sigma_{\mathrm{p}}) = \sigma - \sigma_{\mathrm{p}}, \tag{4}$$

where the compression yield stress $\sigma_{\mathrm{p}} = \sigma_{\mathrm{pi}}(1 + \chi)$ is defined; σ_{pi} is the intrinsic compression yield stress corresponding to the intersection point between compression lines of intact and reconstituted samples; χ is the bonding ratio defined by $\chi = \sigma_{\mathrm{p}}/\sigma_{\mathrm{pi}} - 1$.

The hardening function for σ_{pi} is defined as

$$\sigma_{\mathrm{pi}} = \sigma_{\mathrm{pi0}} \exp\left(\frac{\varepsilon^{\mathrm{p}}}{c_{\mathrm{p}}}\right), \tag{5}$$

where c_{p} is the compression index for the compression curve plotted on $\varepsilon^{\mathrm{p}} - \log\sigma$ plane.

Therefore, the difference between Eq. (4) in the revised model and the original model [15] lies in introducing the inter-cluster bonding by χ for normal compression behavior, as shown in Fig. 1. If the inter-cluster bonding is given by $\chi = 0$, Eq. (4) can be reduced to original model [15].

A damage law was introduced in the expression of bonding ratio at inter-cluster level, expressed as follows

$$\chi = \chi_0 \exp(-\xi_{\mathrm{n}} \varepsilon^{\mathrm{p}}), \tag{6}$$

where χ_0 is the initial bonding ratio; ξ_{n} is the factor of damage representing the influence of normal displacement in the damage law. Therefore, during loading each contact produces a progressive damage of bonding ratio. For $\chi_0 = 0$, the equation can be reduced to that used in Ref. [15].

3.1.3 Influence of density state on the phase transformation angle ϕ_0

Burland et al. [2] reported results of drained and undrained triaxial tests on reconstituted and intact samples of stiff clays. For over-consolidated samples, the clay dilates starting from a stress ratio (phase transformation line) much lower than the critical state line from reconstituted samples. Based on this fact, in this approach, we propose that the local phase transformation line $\tan\phi_0$ depends not only on the internal friction angle ϕ_μ, but also on the density state, expressed as

$$\tan\phi_0 = \left(\frac{e_c}{e}\right)^{-m} \tan\phi_\mu, \tag{7}$$

where m is a material constant to control the slope of phase transformation line. The same value of m as that for resistance shown in Ref. [15] is used for simplification. This relationship allows a dense packing to dilate at earlier stage of shear loading.

Note that one of important elements to consider in granular modeling is the concept of critical state, thus the influences of interlocking and rolling friction of interparticles on the mechanical behavior of the assembly can be dealed with by introducing this concept using Eq. (7) and Eq. (18).

3.2 Determination of model parameters

The model involves the following parameters which can be determined from two isotropic or K_0 compression tests (one for intact sample, the other for reconstituted sample) combined with one undrained compression test:

(1) Contact number per unit volume N/V and mean cluster size d

The mean size d of the clay clusters was assumed to be $4\,\mu$m [15], and the value of $N/V = 12/[\pi d^3(1 + e)e]$ is obtained using size d and void ratio e. Thus, no input is needed.

(2) Inter-cluster elastic constants: k_{n0}, k_{rR} and n

The exponent $n = 1$ is generally assumed to obtain a linear rebound line in e–lg p' plane. $k_{\mathrm{rR}} = 0.5$ can be generally assumed for clay. $k_{\mathrm{n0}} = 9(1 + e_0)\sigma_{\mathrm{at}}/4\kappa$ (the atmosphere pressure $\sigma_{\mathrm{at}} = 101.325\,\mathrm{kPa}$) can be calculated by using rebound index κ measured from the rebound curve of isotropic compression. Therefore, only κ and initial void ratio e_0 is needed as input parameter.

(3) Inter-cluster plastic shear stiffness ratio k_{pR}

According to the hardening rule used for shear sliding, the k_{pR} determines the curve of shear stress–strain. Thus, for a given stress–strain curve the k_{pR} can be obtained from shear stress–strain curve fitting.

(4) Inter-cluster friction angle: ϕ_μ and m

The ϕ_μ is assumed equal to the internal friction angle of the material. $m = 1$ is generally assumed for clay.

(5) Dilatancy constant D

The parameter D influencing the magnitude of dilatancy can be determined from undrained stress path or drained volumetric change behavior.

(6) Inter-cluster plastic normal compression: σ_{pi0}, c_{p}, χ_0 and ξ_{n}

The σ_{pi0} can be measured from intersection point ($\sigma_{\mathrm{pi0}} = p_{\mathrm{pi0}}$ on global curve in e-log p' plane) of compression lines between reconstituted and intact samples. The $\chi_0 = p_{\mathrm{p0}}/p_{\mathrm{pi0}} - 1$ can be obtained with compression yield stress p_{p0} measured from the compression line of intact sample. Since $c_{\mathrm{p}} = (\lambda - \kappa)/3(1 + e_0)$ can be obtained using compression index λ and rebound index κ of an assembly of clay clusters, we use λ as input parameter instead of c_{p}. The ξ_{n} controls the debonding rate of χ. Thus, for a given compression curve the ξ_{n} can be obtained (see discussion later, Fig. 4).

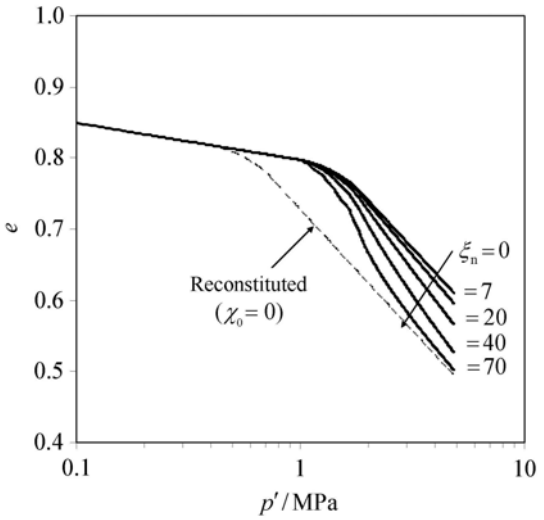

Fig. 4 Predicted behavior of one-dimensional compression

(7) Inter-cluster cohesive stress: σ_{b0} and ξ_d

The parameters σ_{b0} and ξ_d can be obtained by curve fitting from one undrained triaxial test (see discussion later, Fig. 5).

(8) Critical state line: e_{cr0}

The e_{cr0} can be measured from critical state line in e–lg p' plane corresponding to p_{ref} = 100 kPa.

3.3 Model performance for behavior description

The performance of the model is examined under different conditions using the model constants given in Table 1. First, a one-dimensional compression test is considered. Model simulations using different values of damage parameter ξ_n are shown in Fig. 4. In this figure, the general compression behavior shown in Fig. 1 can be reproduced. The destructuration process is simulated depending on its destructuration rate which is related to the damage parameter ξ_n. Based

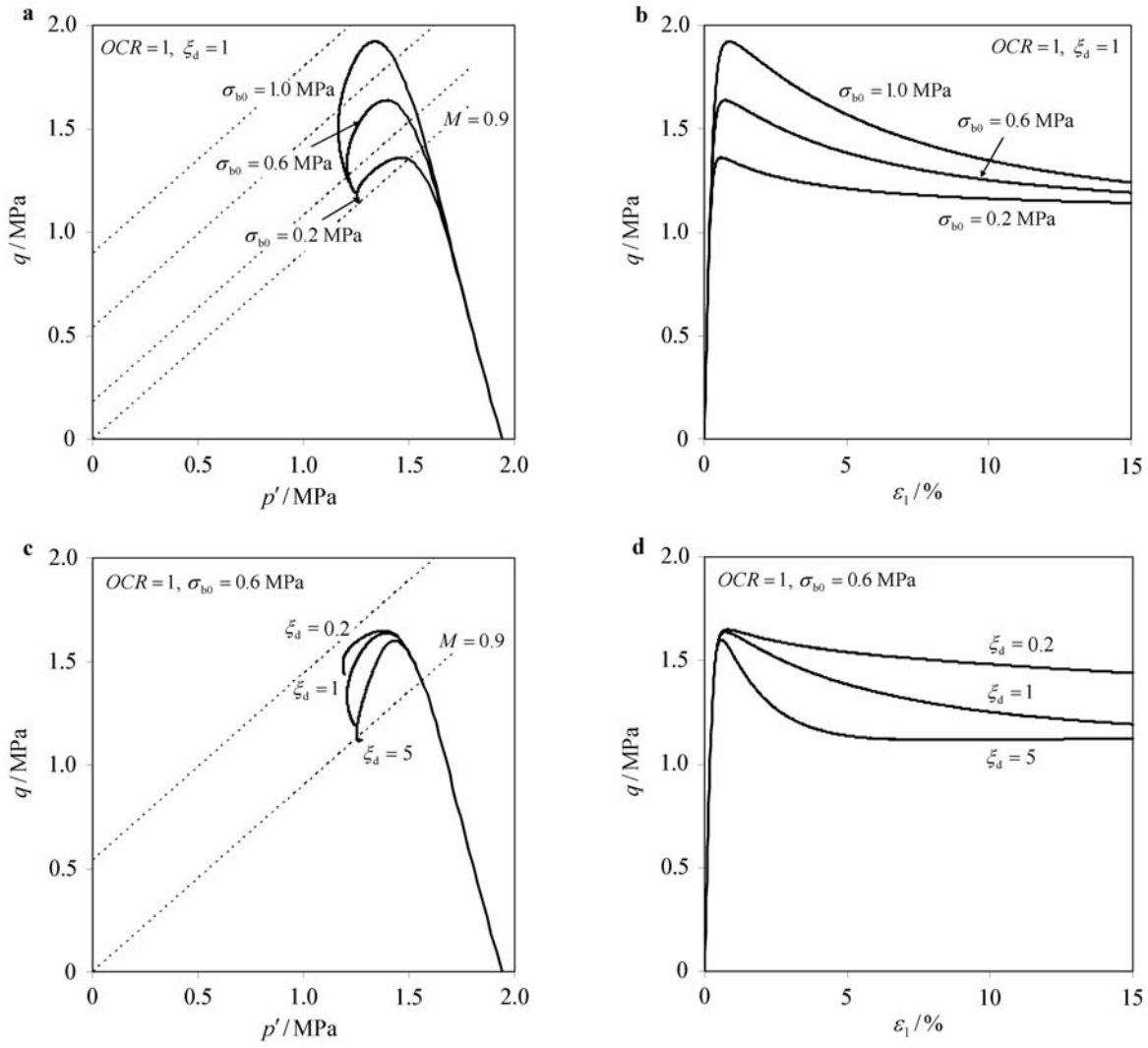

Fig. 5 Predicted behavior of undrained triaxial tests: **a**, **b** Effect of initial cohesion; **c**, **d** Effect of damage factor; and **e**, **f** Coupling effect of initial cohesion and damage factor

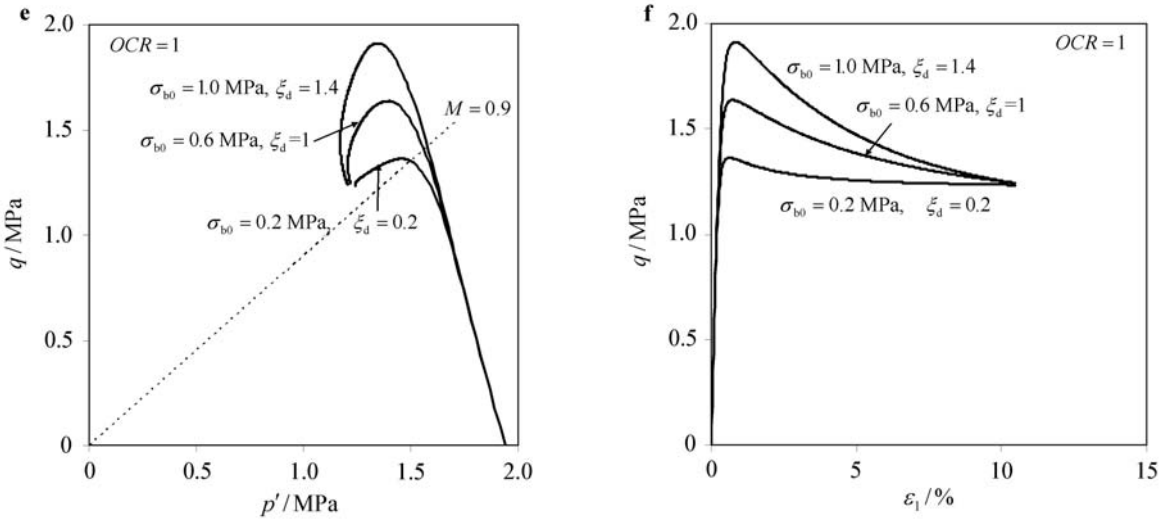

Fig. 5 Predicted behavior of undrained triaxial tests: **a**, **b** Effect of initial cohesion; **c**, **d** Effect of damage factor; and **e**, **f** Coupling effect of initial cohesion and damage factor (continued)

on this result, different values of ξ_n can be determined for different stiff clays.

Table 1 Values of parameters for Vallericca clay

Global parameters				Inter-particle parameters								
κ	λ	e_0	e_{cr0}	D	ϕ'_μ	k_{rR}	k_{pR}	σ_{pi0}	χ_0	ξ_n	σ_{b0}	ξ_d
0.022	0.148	0.84	1.1	1	23°	0. 5	0.8	550	1.55	7	600	1

Then an undrained triaxial test on normally consolidated sample was selected for the simulation, as shown in Figs. 5a and 5b for a given $\xi_d = 1$ with different values of σ_{b0} (200 kPa, 600 kPa and 1 000 kPa), and in Figs. 5c and 5d for a given $\sigma_{b0} = 600$ kPa with different values of ξ_d (0.2, 1 and 5). The initial cohesive stress σ_{b0} controls the magnitude of peak strength and ξ_d controls the destructuration rate of cohesive stress for intact clay, as their definitions. Figures 5e and 5f show coupling effect of σ_{b0} and ξ_d. Different values of (σ_{b0}, ξ_d) can be selected to obtain the same stress level at an axial strain of 10% but with different stress evolutions during straining. According to this suggestion, σ_{b0} and ξ_d can be obtained from the measured stress–strain curve of intact sample.

4 Test simulations

4.1 Review of experimental results

The applicability of the model is investigated by comparing its predictions with the results of a series of laboratory tests on Vallericca stiff clay [1, 9, 12]. The selected triaxial tests are distinguished in two types: medium-pressure (MP) tests for values of p'_{max} lower than the yield stress p_{p0} (see Fig. 6) and high-pressure (HP) tests where $p'_{max} > p_{p0}$. In all selected tests, anisotropic compression and swelling paths were applied to the natural samples before shearing. Samples were then sheared or anisotropically swelled back to different OCRs prior to shearing.

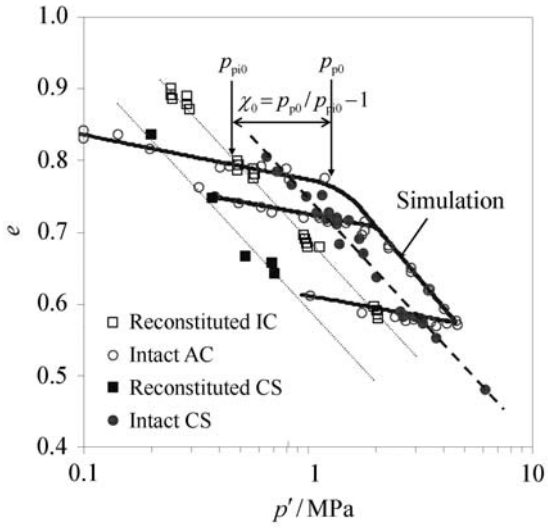

Fig. 6 Compression curves and critical states for intact and reconstituted samples of Vallericca clay

Amorosi and Rampello [9] also gave isotropic compression line and critical state line from tests on reconstituted samples, as shown in Fig. 6. The critical state line of intact clay samples is very different from that of reconstituted samples. This is different from soft sensitive clay which has a unique critical state line for intact and reconstituted samples.

4.2 Calibration of model parameters

Isotropic and anisotropic compression tests (see Fig. 6) and one undrained triaxial test (see MP: $OCR = 1$ in Fig. 7) were used to determine parameters. Parameters κ, λ, e_0, e_{cr0}, σ_{pi0}, χ_0 were measured from Fig. 6 with ξ_n obtained from destructuration rate (see Fig. 4). $\phi_\mu = 23°$ was obtained from triaxial tests on reconstituted samples (see Fig. 2c by Ref. [2]). $k_{pR} = 0.8$ was obtained from fitting stress–strain curve at small strain range where the influence of destructuration is very slight (as shown in Fig. 5). $D = 1$ was obtained from fitting the effective stress path of undrained test. σ_{b0} and ξ_d were obtained from fitting the stress–strain curve of undrained test (according to the method shown in Figs. 5e and 5f). All values of parameters are summarized in Table 1 which will be used to simulate other tests on the same material.

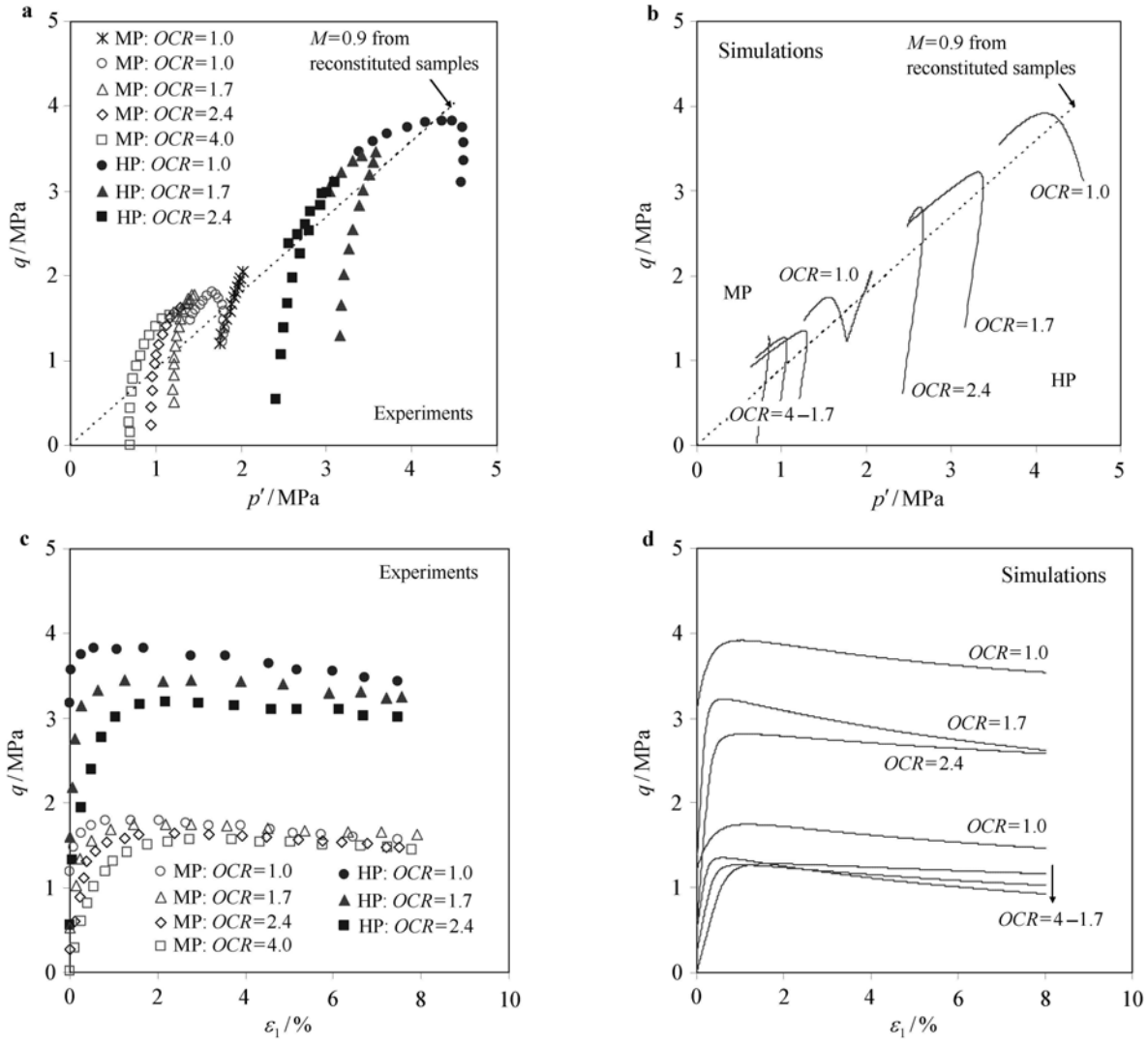

Fig. 7 Comparison between experimental and simulated results for undrained triaxial tests on Vallericca clay: **a**, **b** Effective stress paths; and **c**, **d** Deviatoric stress versus axial strain

4.3 Test simulations and comparisons

For each of the MP and HP tests, the proposed model was used to simulate the complete sequence of consolidation, rebound and shearing stress paths followed by the specimen-test in the laboratory. In particular, the simulations were performed under stress-controlled conditions during the consolidation and rebound stages of the tests, followed by the

strain-controlled shearing stage.

Figure 6 shows the comparison between experimental results and simulations for the anisotropic compression test. Good agreement is achieved, as respected for parameters determination.

Figure 7 shows the comparisons for all selected undrained triaxial tests with different OCRs. Figure 8 shows the prediction for drained triaxial on normally consolidated clay, for which the effective stress path can be found in Fig. 7. The volumetric strain behavior of the stiff clay is then examined. In general, simulated results agree with measured ones, although discrepancies were found for some of tests which are probably due to the variation of intact samples since all tests need 7 individual samples. Also we note that the predictions are not worse than those in Ref. [12]. The model well captured the trend of destructuring behavior of stiff clay due to the destructuration process during shearing under various conditions.

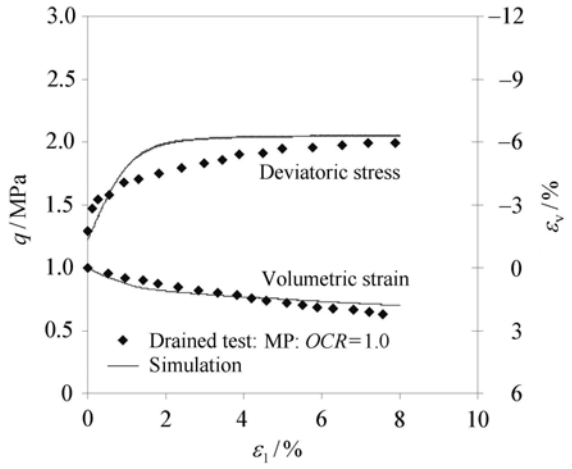

Fig. 8 Comparison between experimental and simulated results for drained triaxial test on Vallericca clay

5 Micromechanical analysis for induced anisotropy and debonding

In this section, we investigate the predicted local stress–strain behavior for selected contact planes with inclined angles θ = 0°, 18°, 28°, 45°, 55°, 72° and 90° (see Fig. 3). The undrained triaxial tests on sample with OCR = 1 under high pressure were discussed as an example for the local behavior of contact planes. In order to study the stress-induced anisotropy during undrained shearing, we have selected three steps: begin of loading, peak deviatoric stress and end of loading.

Figure 9a shows the local stress paths for all selected contact orientations. For the 0° and 90° contact planes, shear stress is null. The stress state with the highest stress ratio is on the 55° contact plane. Figures 9b and 9c show local shear stress–strain curves, which clearly indicates that every contact plane is mobilized to a different degree. The planes with the largest movements are near the orientation of 55° (close to $\pi/4 + \phi_\mu/2$ = 56.5°). These active contact planes contribute largely to the overall deformation of the specimen. Among all selected contact planes, only the 55° contact plane behaves local shear strain softening similar to the global one.

The degradation of bonding ratio and degradation of cohesive stress for all selected contact planes are plotted versus global axial strain in Fig. 10. For cohesive stress (Fig. 10a), most degradation is taken place on the 55° contact plane due to its largest movements. Other contact planes have slight debonding since their mobilized strains are small. For bonding ratio (Fig. 10b), different contact planes have different initial bonding ratios due to the debonding during previous anisotropic compression. During undrained shearing, the 90° contact plane has no debonding since there is only unloading process in normal direction. Among other contact planes, slight degradation is taken place on the 55° contact plane due to its movements by shear induced dilatancy, and other contact planes have very slight debonding during the beginning of shearing and stop debonding at certain global strain levels (from 0.5% to 1.4%).

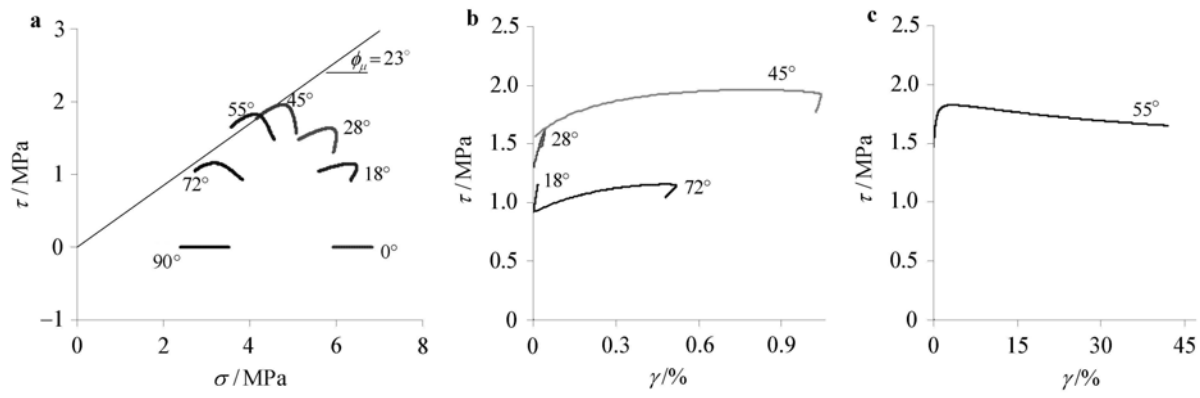

Fig. 9 Local behavior on selected inter-cluster planes for the selected undrained triaxial test: **a** Local stress path; **b**, **c** Local shear stress versus shear strain

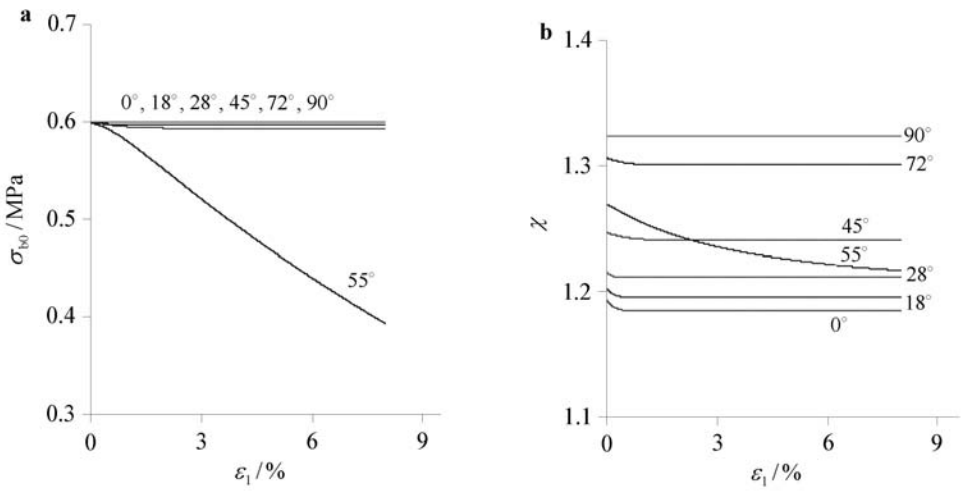

Fig. 10 Local debonding on selected inter-particle planes during undrained shearing: **a** For cohesion; **b** For bonding ratio

In the present model, the inter-cluster bonding on each plane are considered as internal state variables, and their evolution can serve to model the behavior change on each individual plane, thus the results exhibit naturally the induced anisotropy of debonding.

6 Conclusions

Cementations formed in geological timescale were observed in various stiff clays. The bonding and debonding effects on the stress–strain behavior of stiff clay were investigated. Based on this, a micromechanical stress–strain approach has been developed for modeling the behavior of stiff clay. In this model, the clay cluster is considered as particle. The model is based on the description of inter-cluster contact law which requires a simple local stress–strain relation on a contact plane.

The inter-cluster bonding of stiff clay was considered explicitly in the model at each cluster contact, including shear cohesive stress giving an amount of cohesion in shear sliding and normal bonding ratio enlarging the normal yield stress. Damage laws for inter-cluster bonding were proposed at each cluster contact for the debonding process during mechanical loading. The intensity of the damage was taken as a function of the local plastic strains of two contacting clusters.

Undrained and drained triaxial tests on Vallericca stiff clay were simulated to evaluate the present model. Comparisons between experimental results and simulations demonstrate the model's capability of describing correctly the destructuring behavior of stiff clay including induced anisotropy.

The predicted behavior of contact planes has been examined for an undrained triaxial test on sample with $OCR = 1$. The local stress–strain response on contact planes has shown that every contact plane is mobilized to a different degree. A few active contact planes contribute largely to the deformation of the assembly, while most contact planes are inactive and have small movement. Therefore, the local stresses and strains are highly non-uniform, implying the development of anisotropy (e.g. distributions of soil properties: elastic and plastic modulus, bonding) induced by the externally applied load.

Acknowledgement Authors thank Prof. Ming-Jing Jiang at Tongji University for his support.

References

1 Rampello, S., Georgiannou, V.N., Viggiani, G.: Strength and dilatancy of natural and reconstituted Vallericca clay. In: Proc. Int. Symp. on Hard Soils–Soft Rocks, Athens 1, 761–768 (1993)
2 Burland, J.B., Rampello, S., Georgiannou, V.N., et al.: A laboratory study of the strength of four stiff clays. Geotechnique **46**(3), 491–514 (1996)
3 Cotecchia, F., Chandler, R.J.: The influence of structure on the pre-failure behaviour of a natural clay. Geotechnique **47**(3), 523–544 (1997)
4 Kavvadas, M., Anagnostopoulos, A.: A framework for the mechanical behaviour of structured soils. In: Proc. 2nd Int. Symp. Hard Soils–Soft Rocks, Naples 2, 603–614 (1998)
5 Cotecchia, F., Chandler, J.: A general framework for the mechanical behaviour of clays. Geotechnique **50**(4), 523–544 (2000)
6 Cafaro, F., Cotecchia, F.: Structure degradation and changes in the mechanical behaviour of a stiff clay due to weathering. Geotechnique **51**(5), 441–453 (2001)
7 Rampello, S., Calabresi, G., Callisto, L.: Characterisation and engineering properties of a stiff clay deposit. In: Proceedings of the International Workshop on Characterisation and Engineering Properties of Natural Soils, Singapore, 2, 1021–1045

(2002)
8 Jovicic, V., Coop, M., Simpson, B.: Interpretation and modelling of deformation characteristics of a stiff North Sea clay. Canadian Geotechnical Journal **43**(4), 341–354 (2006)
9 Amorosi, A., Rampello, S.: An experimental investigation into the mechanical behaviour of a structured stiff clay. Geotechnique **57**(2), 153–166 (2007)
10 Lagioia, R., Nova, R.: Experimental and theoretical study of the behaviour of a calcarenite in triaxial compression. Geotechnique **45**(4), 633–648 (1995)
11 Gens, A., Nova, R.: Conceptual bases for a constitutive model for bonded soils and weak rocks. In: Proc. Int. Symp. Hard Soils–Soft Rocks, Athens 1, 485–494 (1993)
12 Kavvadas, M., Amorosi, A.: A constitutive model for structured soils. Geotechnique **50**(3), 263–273 (2000)
13 Liu, M.D., Carter, J.: A structured cam clay model. Canadian Geotechnical Journal **39**(6), 1313–1332 (2002)
14 Amorosi, A., Boldini, D., Germano, V.: Implicit integration of a mixed isotropic-kinematic hardening plasticity model for structured clays. International Journal for Numerical and Analytical Methods in Geomechanics **32**(10), 1173–1203 (2008)
15 Chang, C.S., Hicher, P.Y., Yin, Z.Y., et al.: Elastoplastic model for clay with microstructural consideration. ASCE Journal of Engineering Mechanics **135**(9), 917–931 (2009)
16 Yin, Z.Y., Chang, C.S.: Microstructural modelling of stress-dependent behavior of clay. International Journal of Solids and Structures **46**(6), 1373–1388 (2009)
17 Yin, Z.Y., Chang, C.S., Hicher, P.Y., et al.: Micromechanical analysis of kinematic hardening in natural clay. International Journal of Plasticity **25**(8), 1413–1435 (2009)
18 Ishihara, K., Tatsuoka, F., Yasuda, S.: Undrained deformation and liquefaction of sand under cyclic stresses. Soils and Foundations **15**(1), 29–44 (1975)